Icarus 282 (2017) 118–126

Contents lists available at ScienceDirect

Icarus

journal homepage: www.elsevier.com/locate/icarus

Experimental investigation of insolation-driven dust ejection from Mars' CO_2 ice caps

E. Kaufmann*, A. Hagermann

Department of Physical Sciences, The Open University, Walton Hall, Milton Keynes, MK7 6AA, UK

ARTICLE INFO

Article history:
Received 19 May 2016
Revised 7 September 2016
Accepted 15 September 2016
Available online 28 September 2016

Keywords:
CO_2 ice
Mars, polar caps
Laboratory experiments
Martian spider formation
Solid state greenhouse effect

ABSTRACT

Mars' polar caps are – depending on hemisphere and season - partially or totally covered with CO_2 ice. Icy surfaces such as the polar caps of Mars behave differently from surfaces covered with rock and soil when they are irradiated by solar light. The latter absorb and reflect incoming solar radiation within a thin layer beneath the surface. In contrast, ices are partially transparent in the visible spectral range and opaque in the infrared. Due to this fact, the solar radiation can penetrate to a certain depth and raise the temperature of the ice or dust below the surface. This may play an important role in the energy balance of icy surfaces in the solar system, as already noted in previous investigations. We investigated the temperature profiles inside CO_2 ice samples including a dust layer under Martian conditions. We have been able to trigger dust eruptions, but also demonstrated that these require a very narrow range of temperature and ambient pressure. We discuss possible implications for the understanding of phenomena such as arachneiform patterns or fan shaped deposits as observed in Mars' southern polar region.

1. Introduction

The Martian polar caps are currently the only assured naturally occurring carbon dioxide ice deposits in the inner solar system and they are one of the most active geological features on the Martian surface. Both polar caps are seasonally covered with CO_2 ice. While at the northern polar cap the CO_2 ice sublimes during the summer season uncovering a base of H_2O ice, there is a perennial and seasonal CO_2 ice deposit at the southern polar cap (Bibring et al., 2004; Langevin et al., 2005). In the areas surrounding the polar caps phenomena that have no terrestrial analogues can be observed. An example is the so-called 'cryptic region', a dark region covered by ice in the southern polar area (Kieffer et al., 2000; Titus et al., 2008). Here, dark surface features can be found that have a low visible albedo, close to that of bare Martian soil, and at the same time a low surface temperature, approximately the sublimation temperature of CO_2 ice - two properties that seem to contradict each other. This 'albedo-temperature paradox' can be explained by the assumption that a large fraction of the solar flux penetrates a layer of CO_2 ice and is absorbed either by the dust underneath or in a dust layer inside the CO_2 ice cover. Another possible explanation for this effect is described by Langevin et al, (2006). They mention that in early spring the CO_2 ice layer is covered by a thin dust layer and that, in case of thermal equilibrium of ice and dust, a similar signature in the temperature and albedo observations would be recorded.

Some of the most dominant features that can be observed in the cryptic region are the so-called arachneiforms, or 'spiders', branching radial troughs or channels diverging from one common centre (e.g. Kieffer et al., 2000; Piqueux et al., 2003; Portyankina et al., 2010, 2012). A possible explanation for the formation of these geomorphic features is the so-called 'solid-state greenhouse effect', further on denoted as SSGE, a phenomenon similar to the atmospheric greenhouse effect (Brown and Matson, 1987; Fanale et al., 1990): sunlight can penetrate the CO_2 ice layer down to a dust deposit at depth where the radiation is absorbed, with the heat increase leading to sublimation of the CO_2 ice on the boundary between the ice layer and the underlying dark material. As gas pressure increases, the overlaying ice fractures where it is weakest, leading to gas ejections that transport entrained dust to the surface. The SSGE was also considered as a possible explanation for geyser–like eruptions observed on Triton by Voyager 2 (see Soderblom et al., 1990).

A number of researchers have explored the theoretical aspects of this topic (e.g. Matson and Brown, 1989; Fanale et al. 1990; Portyankina et al., 2010). However, only few results of laboratory measurements of sub-surface heating caused by irradiation could be found in literature (see e.g. Dissly et al., 1990; Kaufmann et al., 2006).

* Corresponding author.
E-mail address: erika.kaufmann@open.ac.uk (E. Kaufmann).

http://dx.doi.org/10.1016/j.icarus.2016.09.039

In a series of experiments, de Villiers et al. (2012) showed that a pressure-gradient-driven gas flow inside granular media can lead to erosion that produces patterns similar to the spider-like structures observed on Mars. This supports the theory that spiders are the results of venting of CO_2 gas. Further laboratory experiments concerning the influence of solar radiation on CO_2 ice and dust have been performed recently by Philippe et al., 2015, but, as far as it is known to the authors, no results from experiments showing the formation and influence of pressure gradients inside CO_2 ice under Martian conditions have been published so far.

Based on work by Kaufmann et al. (2006), who investigated the solid state greenhouse effect on various materials such as clear compact H_2O ice and glass beads with and without absorbing layers, we investigated the behaviour of CO_2 ice under Martian conditions in a series of experiments. These experiments may contribute to our understanding of the phenomena observed on Mars. Note that our aim is not to advance the underlying theory, nor give any quantitative explanation for this phenomenon, which (after careful laboratory simulations) turns out to be a remarkably complex process. However, by presenting the results of a long series of resource-intensive experiments and our interpretation of the phenomena observed, we are hoping to elucidate some of the open questions surrounding the processes taking place in Mars' cryptic region.

2. Laboratory experiments

We have observed the behaviour of CO_2 ice slabs containing a dust layer under insolation in Martian conditions. The measurements were intended to improve our understanding of the phenomena observed in the cryptic regions on Mars, although the CO_2 ice samples were not produced under Martian conditions. Nevertheless, our ice slabs were produced directly from the gas phase. For this purpose, a pressure vessel was continuously flooded with CO_2 gas at a pressure of about 1.5 to 2 bar. The base of the vessel was cooled by immersing it in a bath of liquid nitrogen while the top of the vessel was kept at a temperature above 193 K, i.e. although the partial pressure of the gas is higher than on Mars the temperature during ice deposition is in a similar range. The gas froze from the base upwards, which resulted in blocks of translucent CO_2 ice. This method is based on Behn (1900).

The ice samples are of polycrystalline structure and have an average density of 1570 kg/m^3 ± 110 kg/m^3. They were almost perfectly transparent on mm to cm scales. The large number of cracks and fissures in the ice reduced the transparency but, although the final sample was only translucent, the dust layer inside could clearly be seen, i.e. the light could penetrate down to the dust layer with only very little scattering. The white-ish appearance of our samples in the images is mainly caused by H_2O frost forming on the samples immediately as they were taken out of the chamber. Especially in Fig. 3 the H_2O ice crystals settled can clearly be seen.

Although the pressure during the ice growing process was much higher than on Mars, the samples are still an appropriate starting point for investigations of the solar influence on CO_2 ice layers at the Martian polar caps. The absorbing layers were obtained by adding Mars analogue material (JSC Mars-1A) in different grain size ranges to the samples by pouring a certain amount of dust on the surface of one ice block and putting a second ice block on top of it. The crack between the two blocks was then sealed with ice before the experiment was started.

The basic set-up for all the experiments was the same: a cylindrical block of CO_2 ice, with an initial diameter d_s of 12.5 cm and a height h_s between 6 and 10 cm, including a layer of dust, was put on a cooled base plate in a vacuum chamber. The temperature profile inside the sample during the experiment was measured using RTD temperature sensors (PT100). During the experiments the environmental chamber was cooled down by using liquid nitrogen and a temperature control system to temperatures of 150 K or below and depressurised to values below 10 mbar. The samples were irradiated using a solar simulator[1] and the temperature profile inside the sample was measured whilst ambient pressure was monitored. Additionally, a time lapse record of the morphology of the sample during the irradiation phase was obtained using a set of commercial off-the-shelf webcams. A sketch of the sample preparation and the measurement set-up is given in Fig. 1.

2.1. Measurements using unsorted dust

Samples were prepared by stacking two slabs of CO_2 ice, with approximately 1 g of JSC Mars-1A dust (grain size $d \leq 1$ mm, randomly distributed) centred on the surface of the lower slab. The dust was concentrated within a circle approximately 8 cm in diameter. The two slabs were re-introduced into the pressure vessel, which was then flooded with CO_2 gas whilst being cooled from the base and heated at the top, as outlined above. This procedure leads to a sealing of the gap between the two slabs by resubliming CO_2 gas. The result is a compact sample with a dust layer inside. PT100-sensors were inserted into holes drilled into the ice block with a vertical spacing of 1 cm. It has to be noted that simply inserting sensors into drill holes led to non-optimal thermal contact between the sensors and the sample.

The fundamental conditions for these experiments were identical: the copper base plate was pre-cooled to $T_0 \sim 150$ K. In the following, we will refer to the temperature T_0 of the base plate as 'base temperature'. The pressure inside the environmental chamber was kept at approximately 5.3 mbar and the samples were irradiated with an intensity of 650 Wm^{-2}, an intensity that is higher than at the Martian polar caps, since these experiments were meant to prove the concept that a pressure increase inside CO_2 ice can lead to observable dust eruptions. This leads to a higher energy input within a short time period and therefore reduces the experiment's run time which is constrained by the supply of liquid nitrogen for cooling.

However, the duration of the irradiation phase and the height of the samples varied (see Table 1 for details). During the experiments no additional CO_2 was introduced into the chamber which means that any additional deposition of CO_2 ice on the sample was avoided. The change of the sample was captured from two different angles during the experiment (top view and side view). No signs of dust ejection could be found in the time lapse footage or in the environmental chamber. Neither did careful examination of the samples after insolation suggest that dust had erupted from the slab.

With regard to the SSGE, no definite temperature maximum below the surface could be detected unambiguously and quantitative reproducibility of the temperature recordings was rather poor. This is partly owed to the fact that the *p-T* regime is largely influenced by the sublimation and deposition of CO_2 and the associated exchange of latent heat which affects temperature measurements. Nevertheless, careful examination of the sample after irradiation showed clear evidence of the influence of solar radiation on the temperature of the dust layer. The radiative energy absorbed by the dust had caused the surrounding ice to sublime, with the dust sinking through the ice, leaving a cavity in its wake, as shown in Fig. 2. Ice channels created by the dust particles, or needle-like ice features that remained around those channels were what defined these experiments with a random mix of dust grain sizes. These features could clearly be seen when the sample was cut in half. For dust particles towards the large end of the grain size range, a

[1] LS1000R3 Solar Simulator, Solar Light Company, Inc. including AM0 filter

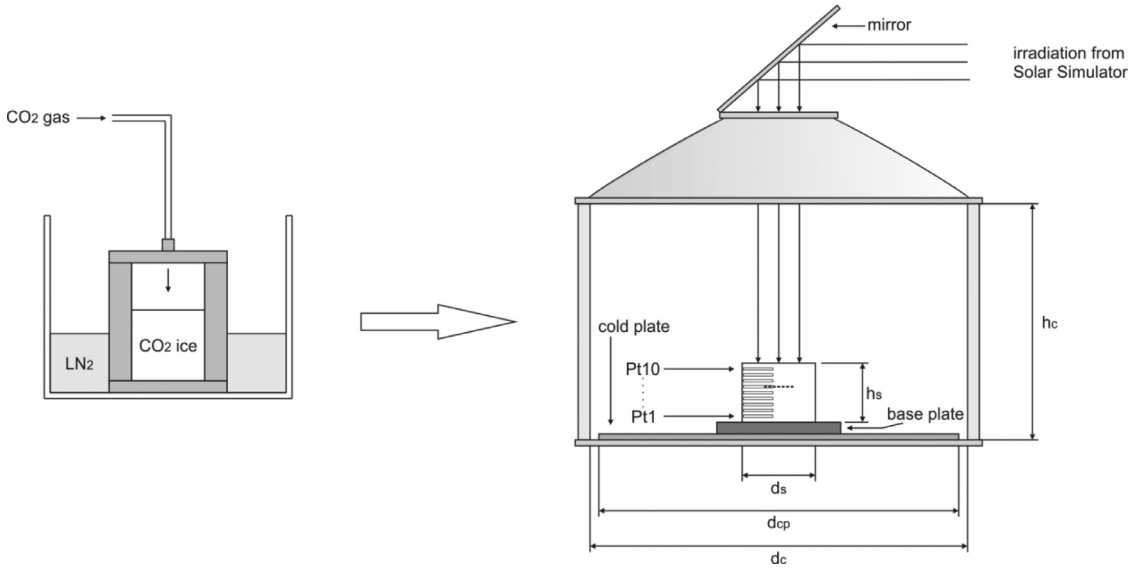

Fig. 1. Left: Sample preparation by flooding a pressure vessel that is cooled with LN_2 from below with CO_2 gas. Right: Our environmental chamber with inner dimensions of height $h_c = 40$ cm and diameter $d_c = 65$ cm. The cold plate at the bottom of the chamber has a diameter of $d_{cp} = 61$ cm and is cooled with LN_2. A squared base plate (copper, side length 21 cm, height 2 cm) is screwed onto the cold plate. The CO_2 ice block set on top of the base plate includes up to 10 sensors (Pt1 to Pt10) with a vertical distance of 1 cm. The dashed line represents the dust layer.

Table 1
Summary of experiments with dust grain size $d \leq 1$ mm: h: initial height of the sample; h_d: initial thickness of ice above the dust layer; p: pressure inside the environmental chamber; T_0: base temperature, i.e. temperature at the copper base plate; T_{min}: minimum temperature measured inside the sample; $z(T_{min})$: distance from the base where T_{min} was measured; t_{ir}: duration of the irradiation phase. A possible explanation why T_{min} differs from T_0 is given in Section 4.

Exp	h [cm]	h_d [cm]	p [mbar]	T_0 [K]	T_{min} [K]	$z(T_{min})$ [cm]	t_{ir} [hrs]	dust ejection
1.1	6.0	3.0	5.3 ± 0.43	152	147.75	1	12.83	no
1.2	7.7	4.7	5.2 ± 0.17	151	148.20	2	14.37	no
1.3	8.5	4.0	5.5 ± 0.27	150	148.57	1	15.88	no

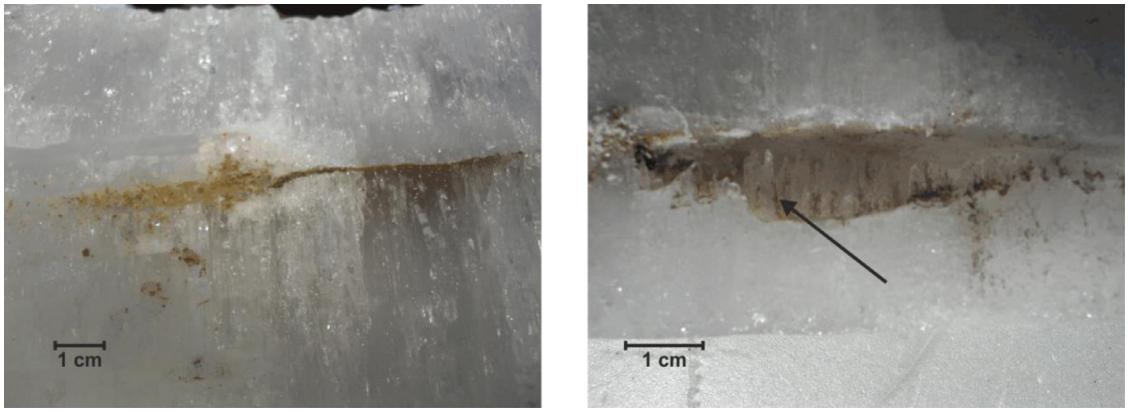

Fig. 2. Left: Dust layer inside a CO_2 ice sample before irradiation. Right: Cavity inside CO_2 ice sample after approx. 14 hours of irradiation. The arrow indicates one of the needle-like ice features that built up in the cavity.

clear downward motion and channel formation could be observed as shown in Fig. 2.

Another effect observed in the experiments was the expansion of the gaps in the ice around the PT100-sensors inserted into drill holes in the ice sample. This may have been caused either by self-heating due to power supplied to the sensors or by radiation being absorbed by the wires.

During none of the experiments with dust grains with a diameter of ≤ 1 mm any evidence of dust eruptions could be observed. A plausible explanation for this would be the lack of sufficient pressure to entrain the dust in any outbursts. Gas could have escaped either through the gaps around the sensors or through spurious cracks and channels around the rather extensive dust layer.

In order to confirm that it is not the gaps around the sensors in the ice that prevent a pressure increase due to sublimation of CO_2 around the dust layer, we ran experiments with no temperature sensors embedded in the ice slab. These are explained in more detail in the next section. In this case, only the temperature at the bottom of the slab was recorded. As for the other experiments, the samples were irradiated for approximately 13 to 15 hours. As before, a cavity had formed by the dust sinking down due to its temperature increase and the sublimation of the surrounding CO_2 ice.

Table 2
Summary of the experiments with dust grains ≤53 µm. No temperature measurements during experiments 2.8, 2.9 and 2.10.

Exp	h [cm]	h_d [cm]	p [mbar]	T_0 [K]	T_{min} [K]	$z(T_{min})$ [cm]	t_{ir} [hrs]	dust ejection
2.1	9.5	4.5	4.84 ± 0.50	149	145.68	2	13.40	yes
2.2	10.5	5.5	4.86 ± 0.25	149	145.90	1	12.00	yes
2.3	9.5	4.5	–	157	143.56	2	14.30	yes
2.4	10.5	5.0	3.60 ± 0.60	156	143.61	3	14.10	?
2.5	10.0	4.5	0.66 ± 0.04	136	133.07	2	12.75	?
2.6	11.0	6.2	4.75 ± 0.17	148	145.68	4	13.85	?
2.7	8.5	3.5	8.10 ± 1.90	159	147.03	1	12.75	no
2.8	10.0	4.0	5.14 ± 0.82	150	–	–	14.83	no
2.9	9.5	4.5	4.30 ± 0.23	148	–	–	12.50	no
2.10	6 to 9	2 to 5	4.15 ± 0.40	148	–	–	12.55	yes

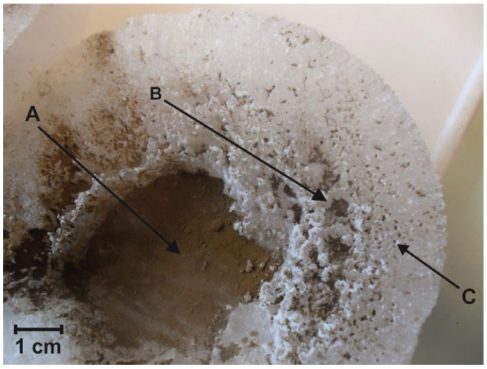

Fig. 3. Cavity and tubes inside CO_2 ice created by heated dust particles subliming their way through the ice matrix (image from Experiment 2.8). A: main area of dust that sank homogeneously during the irradiation phase. B: an example of a pit formed by a bigger agglomeration of dust. C: minor pit created by small agglomeration of dust.

As we were less concerned with monitoring temperatures in this experiment but wanted to facilitate dust ejection, we limited the dust particle size to smaller grains with $d \leq 53$ µm (see also Experiments 2.8 to 2.10, Table 2). For this grain size range, the central region of the dust layer sunk down more homogeneously than the remainder of the dust layer where dust had been scattered more randomly. Here, small vertical tubes had been created by individual or clustered grains (see Fig. 3), but no needle-like structures built up.

2.2. Measurements using fine dust

According to Paige et al. (1994; see also Paige and Keegan, 1994) the average dust particle size across broad areas of Mars' south-polar region is 50 to 200 µm. In order to facilitate particle lifting by flowing gas, a grain size at the lower end of this range ($d \leq 53$ µm) was chosen. Note that this is also the size range de Villiers et al., (2012) used for their experiments. As before, the grain size distribution within the range was random and 1 g of dust was added to the sample. A good seal of the interface where the dust layer is located was seen as essential to facilitate an insolation-induced pressure increase. In order to avoid gas leakage at the interface between the ice slabs, the dust layer was contained in a small region in the centre of the slab. This was achieved by subliming a small depression with a diameter of 5 cm into the lower ice slab. This depression was then filled with dust. Furthermore, the set-up for the next series of experiments was modified as outlined below.

As thermal contact between the PT100 sensors and the ice had been identified as poor, the sample preparation was changed. As before, two slabs of clear CO_2 ice were prepared. Holes were then drilled into the individual slabs and the sensors were placed inside drill holes. One sensor was fixed at or close to the dust layer before the combined sample was reintroduced into the pressure vessel. The vessel was sealed and flooded with CO_2 gas while being cooled down. This ensured that the drill holes and the gap between the two ice-slabs were filled up with ice. The result was a much better thermal contact between the sensors and the ice. The measurements themselves were conducted in the same way as before: the sample was irradiated with 650 Wm^{-2}. Even this improved set-up could not prevent small gaps from forming around the upper sensors. However, these turned out to be much narrower and the lower sensors were still frozen solid in the sample at the end of the experiments. A summary of this experimental series is given in Table 2.

During most of these experiments not only the formation of a cavity, but also some type of dust ejection could be observed. For some of the samples with fine-grained dust layers (i.e. $d \leq 53$ µm), fan-shaped dust deposits were visible on the floor of the environmental chamber. Two examples of such dust deposits are shown in Fig. 4.

Those dust deposits were usually located close to the thermal sensors (and directed towards the vacuum pump flange), which is why thermal sensor self-heating and some minor motion of the sensors due to escaping gas might have played a role in their origin. However, the fan-like dust deposits could already be identified in the time lapse footage before the sensors were removed from the sample. The most plausible explanation is that, as the gap in the ice grows around the thermal sensors, this part of the ice slab is weakened and gas can escape more easily. As mentioned in the former section we also repeated experiments in this series without temperature measurements to rule out any kind of influence of the thermal sensors and recorded the temperature at the bottom of the sample only (Experiment 2.8 to Experiment 2.10 in Table 2).

Although images taken after chamber opening and time lapse footage do not always show clear evidence of a dust eruption such as a dust fan, a small amount of dust which is indicative of an eruption was found in the chamber in three cases. These experiments are indicated with a question mark in Table 2.

As outlined in Table 2, not every experiment resulted in an eruption of dust. In the following we are going to offer a few plausible explanations as to why these events were so difficult to reproduce.

In Experiment 2.7 the upper ice slab broke in halves during sample preparation. As cracks in the CO_2 ice are generally filled during production of the composite slab containing the dust layer, the slab was still used. As expected, cracks, drill holes and any gap between the original ice slabs were sealed. However, not enough care was taken to ensure sufficient homogeneity of the sample. As a result, fissures formed along the re-sealed fracture lines, allowing the gas emanating from the dust layer to slowly escape. Without a pressure increase in the dust layer there can of course be no dust eruption.

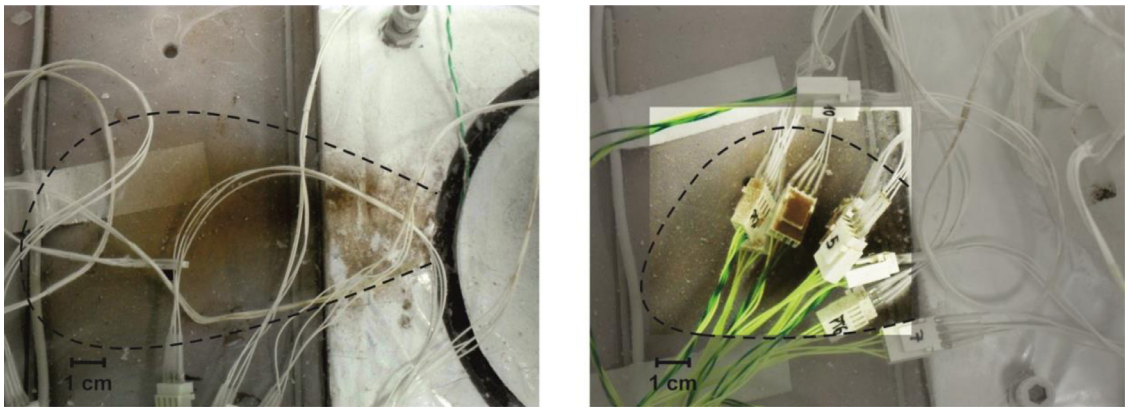

Fig. 4. Images of fan-shaped dust deposits from two different experiments. Left: Experiment 2.1 (l∼11 cm, d∼6 cm), right: Experiment 2.3 (l∼ 10 cm, d∼5 cm) where l is the length of the deposit measured from the rim of the sample, and d stands for the width of the deposit at its broadest extend. Images taken after the vacuum chamber was opened.

No dust ejection could be observed during Experiment 2.8. However, the time lapse record shows that, after several hours of irradiation, dust can be seen falling down the sides of the sample and a horizontal gap grew at the interface between the two sub-slabs. Apparently gas could escape through the gap between the two sub-slabs because the seal was imperfect.

For Experiment 2.9, a different method to cover the dust layer with CO_2 ice was tested. Here, the original ice cylinder was not cut. A depression was sublimed into the cylinder using a heated aluminium cylinder. This depression was then filled with dust. The dust layer was then covered with crushed ice and sealed in the usual way. This kind of sample preparation may have led to more thin cracks in the upper part of the sample on top of the dust and therefore, more gas could escape. Consequently, the pressure increase at the dust layer was not high enough for a dust eruption.

As summarized in Table 2, we have not been able to reproduce sample height accurately. However, the initial thickness of the ice slab above the dust layer is in the range of 5 cm ± 0.5 cm for all experiments where dust eruptions could clearly be observed. Because the temperature gradient below the dust layer is rather smooth, small variations in the exact distance of the ice layer as measured from the base plate is unlikely to influence the results.

3. Observation of a Mars-like dust eruption in the laboratory

Since evidence or traces of eruptive activity could be found after having completed some of the experiments but could not always be clearly seen in the footage, a third camera was added to the set-up to obtain a more 3-dimensional view. This set-up improvement finally made it possible to observe and record a gas driven dust ejection.

During one of our experiments (Experiment 2.10), dust could be observed seeping from the ice slab, a process starting after about 5.5 hours of irradiation. The deposit that formed next to the ice block can be seen on the right hand side in Fig. 5. As discussed by Kieffer et al. (2006), the gas can be released at weak spots either in an explosive or continuous way. The latter seems to be the case in this experiment with its slow but continuous ejection of dust observed. The channel where the dust started seeping was below the merger surface of the two ice slabs making up the sample and directed towards the vacuum pump flange of the chamber.

A small channel from the dust layer towards the surface was noted after an irradiation phase of 12.55 hours, the nominal end of the experiment. Due to a malfunction during sample preparation the sample used in this experiment turned out to be a sloped, truncated cylinder and the channel formed towards the lower side

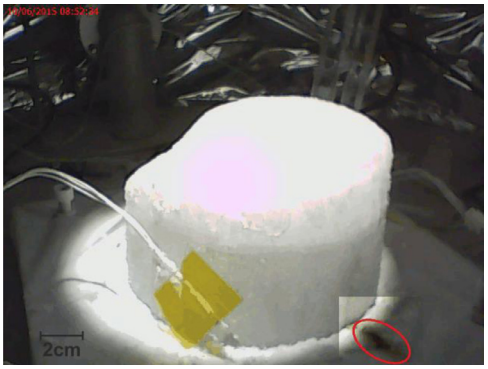

Fig. 5. Dust deposit obtained from dust seepage. The deposit, visible at the lower right of the ice block, was approximately 2 cm long and about 0.7 cm at its broadest extent, so much smaller than the fan-shaped deposits seen for the other experiments. The picture was taken at the end of the first irradiation phase.

of the sample. To facilitate the channel formation leading to a dust eruption on the surface, the sample was reintroduced into the chamber and irradiated once more. There was no active cooling, thus enabling the temperature to rise slowly and steadily. Irradiation was terminated after 3.5 hours, when the temperature at the bottom of the sample had reached 193 K. Pressure was permitted to rise in line with the temperature increase, i.e. for this extended experiment a change in environmental conditions was intended. The values given in Table 2 refer to measurements before the experiment. The original dust layer was 4 cm above the base of the ice slab. Approximately 35 minutes after the irradiation had restarted, an explosive dust ejection originating from the very channel that had started to form during the first irradiation phase, could be observed during the extended experiment, resulting in a fan-shaped dust deposit next to the sample (see Fig. 6).

Additionally, a slow dust ejection could be observed on the surface of the sample, although the amount of dust settling on the surface of the slab was marginal; parts of it fell back into the channel and some was blown away.

4. Temperature profiles of CO_2 ice samples

Although the complexities of sample preparation brought about a certain degree of inhomogeneity in the samples, all experiments that included temperature profile measurements had one thing in common: temperatures recorded by the sensors close to the sample bottom were lower than the base temperature T_0, which was regulated and intended to be our ‘set temperature’. The minimum

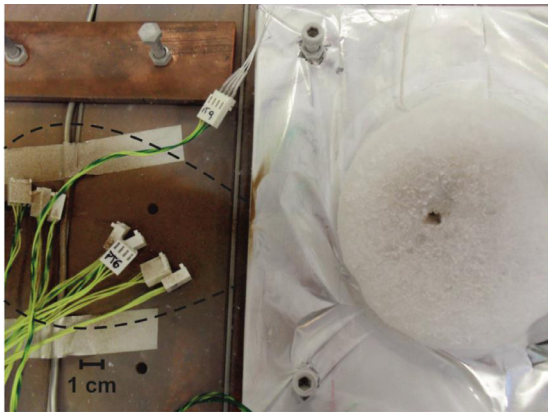

Fig. 6. Fan-shaped dust deposit obtained by an explosive dust eruption from the side of the ice slab and vertical channel seen on the top surface of the sample. The fan was about 15 cm long and about 7.5 cm at its widest extent. Note that minor dust deposits on the surface of the ice block are covered by water ice frost forming after opening of the environmental chamber.

temperature 2 cm above the bottom was about 3.3 K lower in Experiment 2.1, for example, but note that quantitative reproducibility was rather poor. This is not surprising, given that all temperature measurements in this regime are affected by the latent heat conversion related to the sublimation and deposition of CO_2 ice around the temperature sensor. Relevant temperature values and depths are listed in Table 2. Two examples of temperature profiles are given in Fig. 7. Generally (and unsurprisingly), the temperature increase ΔT measured inside the dust layer was higher than the temperature increase measured 1 cm above the dust layer. The temperature curves for Experiments 2.1 and 2.2 were chosen because these experiments have almost identical initial conditions and in both cases a dust eruption could be observed. They also show how large the variation in recorded temperatures is, although the basic parameters are very similar.

Two examples for ΔT-profiles are shown in Fig. 8. As before, two experiments with visible dust eruptions were chosen. In this case the initial conditions were different but the curves show that the dust layer temperature increases more than the temperature of the sensor positioned 1 cm above the dust layer. A possible explanation for the increase and decrease in the temperature measured 5 cm from the base plate in Experiment 2.2 is that the sensor has lost contact to the ice, i.e. a cavity is formed and the sensor does not measure the temperature of the ice or the dust but rather the temperature of the gas or its own self heating.

Figs. 7 and 8 show the general behaviour of the temperatures measured but they also illustrate the difficulty in measuring temperatures reproducibly.

Given the scale of the experiments combined with the complexities of sample preparation, exact reproducibility will be very hard to achieve. However, we believe that the most important factors affecting reproducibility are the environmental conditions. We found there to be a correlation between the minimum temperatures measured inside the sample and the pressure inside the chamber, which is related to equilibrium between the solid and gaseous phase of CO_2 (see Fig. 9).

We compared the combination of pressures and minimum temperatures measured in the laboratory with Martian values returned by the Mars Climate Data Base (http://www-mars.lmd.jussieu.fr/mcd_python/#). Our results are in the same range as surface temperature and surface pressure at a location informally known as

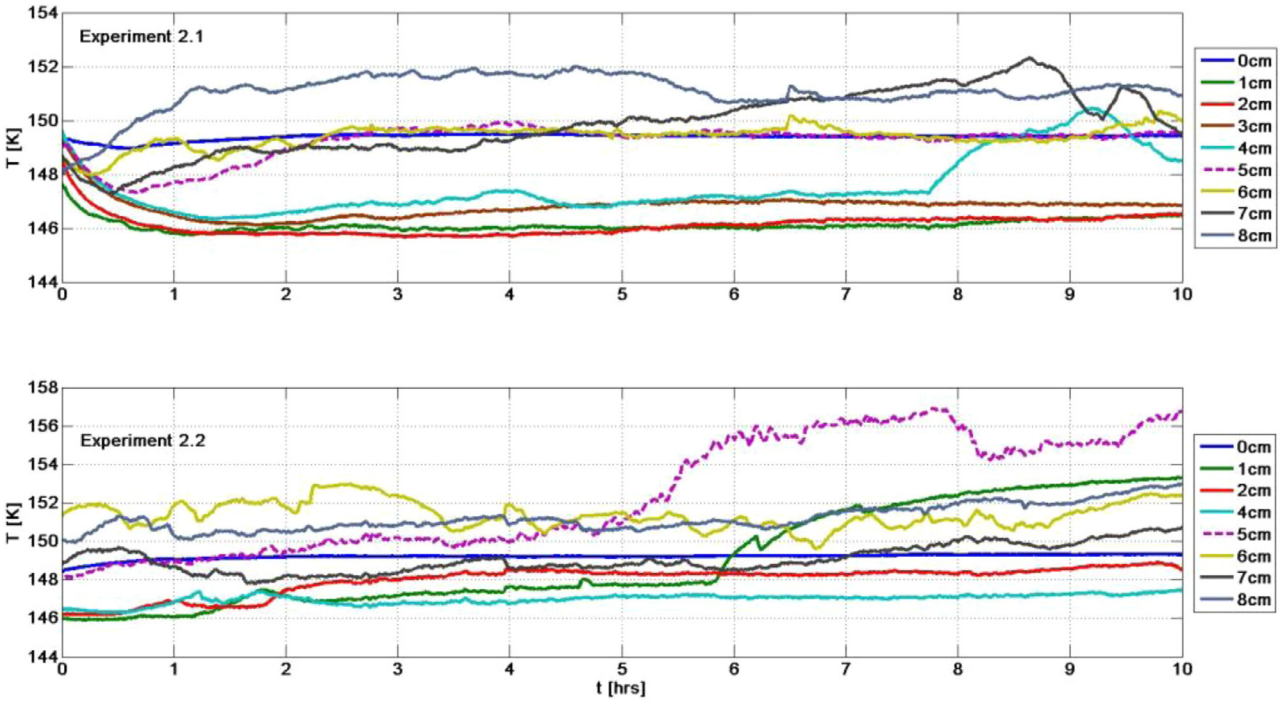

Fig. 7. Temperature histories at various heights above the base plate measured during Experiments 2.1 and 2.2. In both cases the base temperature T_0 (0 cm) was approx. 149 K. The minimum temperatures inside the sample were measured about 1 to 2 cm above the base plate. The dust layer was about 5 cm from the bottom of the sample (dashed line). As pointed out in the text, it is difficult to quantify the actual error of the temperature measurements reliably, although sensor specifications alone suggest an accuracy better than 0.45 K.

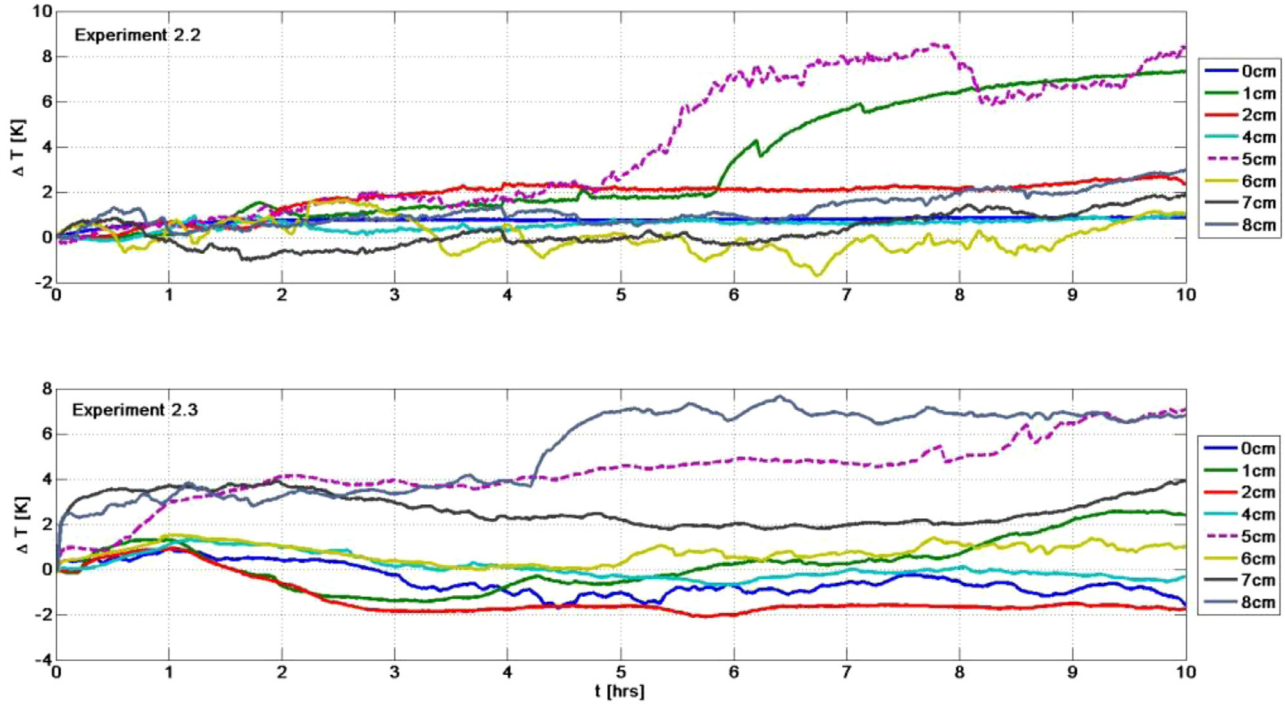

Fig. 8. ΔT histories measured during Experiment 2.2 and 2.3. The dust layer was about 5 cm from the bottom of the sample (dashed line). Although the base temperature was different in the two experiments in both cases the temperature increase inside the dust layer was larger than the temperature increase 1 cm above the dust layer.

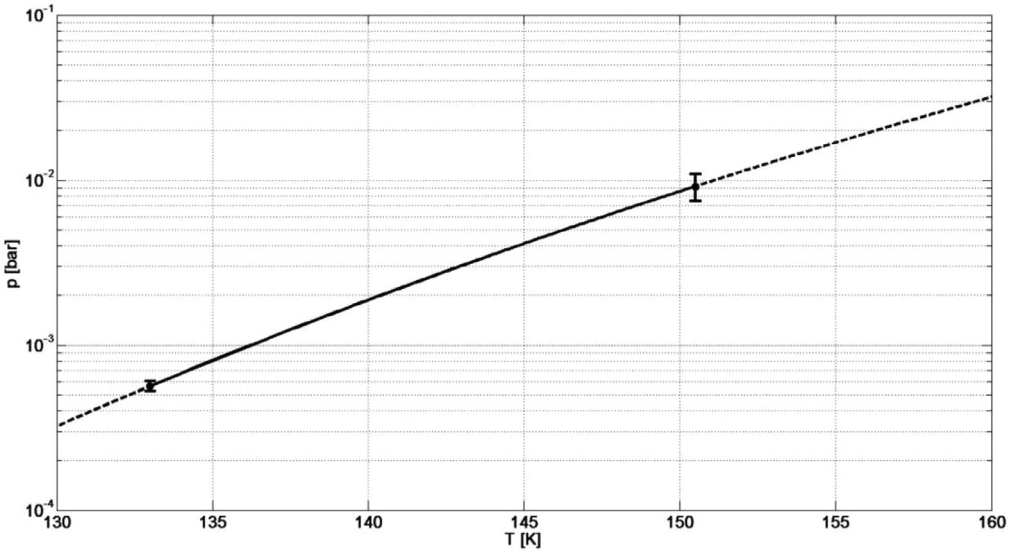

Fig. 9. CO_2 vapour pressure from solid after Meyers and Van Dusen (1933). The solid part of the (otherwise dashed) curve indicates the temperature range of our experiments. Error bars mark the pressure at maximum and minimum temperature as measured.

Manhattan[2] at the time when, according to Thomas et al., (2010), dust driven activity had been observed. Our laboratory measurements have shown that the enigmatic occurrence of surface processes in this latitude band is linked to a unique combination of surface pressure and temperature conditions which cause surface CO_2 ice to become episodically active over the course of a Martian year. Variations in atmospheric pressure seem to play the same role as insolation-driven temperature increases below the ice.

[2] Manhattan is a region within the cryptic terrain (for more details see Hansen et al., 2010).

5. Measurements using active pressure control

All experiments described so far were carried out by evacuating and cooling the environmental chamber, and start irradiating after temperature and pressure had stabilized. At this point the pressure inside the chamber was always lower than the equilibrium pressure for the chosen T_0, the temperature at the sample base.

A third series of experiments with controlled pressure was carried out to establish whether dust activity could occur if pressures inside the chamber equalled or exceeded the equilibrium value for the corresponding base temperatures T_0. Consequently, pressure was kept stable to ensure that it is higher than the equilibrium pressure. To control the pressure it was necessary to let CO_2

Table 3
Summary of the experiments performed with active pressure control. All variables as in Tables 1 and 2.

Exp	h [cm]	h_d [cm]	p [mbar]	T_0 [K]	T_{min} [K]	$z(T_{min})$ [cm]	t_{ir} [hrs]	dust ejection
3.1	6 to 10*	2 to 6*	6.90 ± 2.20	149	148.79	2	07.00	no
3.2	9	4.5	8.75 ± 1.71	150	150.46	0	07.00	no
3.3	9	4.5	3.50 ± 1.90	143	143.02	0	04.60	no

* Slab shape was asymmetrical because of a problem with sample production. The temperature values listed in the table are the mean temperature values at the specified depths.

gas flow into the chamber at a controlled rate. Sample preparation ($d \leq 53$ µm) and set-up remained unchanged. The first experiment of this series differs in that we chose not to pre-cool the CO_2 gas entering the chamber.

For Experiment 3.1 the temperature of the base plate was kept at $T_0 = 149$ K. The pressure was adjusted to be higher than in previous experiments, at approximately 7 mbar, which, according to Meyers and Van Dusen (1933), is still slightly (~0.5mbar) below the equilibrium pressure corresponding to T_0 (see Fig. 9). Once more, the minimum temperature recorded by the two lowermost sensors, was (in this case only marginally) lower than T_0 and, as before, the lowest temperature correlates with the ambient pressure. The highest temperature over the entire experiment duration was recorded closest to the surface.

We conducted two more experiments at different temperatures with pressures above the corresponding equilibrium pressures. The base temperature for Experiment 3.2 was the same as for Experiment 3.1. Given that the vapour pressure of solid CO_2 at 150 K is 8.65 mbar, pressure was regulated to remain slightly above that value, ~8.75 mbar. Similarly the pressure for the third experiment, conducted at a lower base temperature, was regulated to remain above the pressure for $T_0 = 143$ K, $p = 3.1$ mbar. In both cases, a sub-surface temperature maximum could be observed for a certain time (about 30 min for Experiment 3.2 and about 1 h 45 min for Experiment 3.3). As before, quantitative reproducibility remained poor, although we can confidently rule out a temperature decrease inside the sample below T_0. No dust ejection of any kind could be observed. However, cavities still formed around the dust layer in the samples. A summary of the experimental conditions is given in Table 3.

These results are of some significance. Our experiments clearly show how important the balance between pressure and temperature is for the production of dust eruptions. This was confirmed by one additional experiment in which the base temperature T_0 was set to 150 K. Compared with our earlier experiments done at the same base temperature as listed in Table 2 with no active pressure control, this should lead to pressure inside the chamber equilibrating around 5 mbar. Continuous ambient air supply however, kept the chamber pressure around 40 mbar. In contrast to all the other experiments the temperature increase in the dust layer was higher than at any other depth within the sample. Moreover, the temperature curve was smoother than for the other experiments. The sample also showed a different shape after the irradiation phase than the others. No cavity or channel had formed inside the sample.

6. Conclusions

We have reproduced dust eruptions from a layer of dust inside a CO_2 ice slab under Martian conditions. We found that in order to trigger dust eruptions a delicate balance between pressure and temperature near the equilibrium of the CO_2 phase change seems to be necessary.

For all samples with an embedded dust layer a cavity formed inside the sample and the dust layer sagged by approximately 5–10 mm, unless ambient pressure inside the environmental chamber was kept significantly above Martian values. Some samples also showed channels forming from the dust layer towards the sample surface. In some cases a dust ejection could be observed and a fan shaped deposit pattern could be seen on the bottom of the chamber. The eruption occurred at the weakest part of the ice slab, generally on the sides and not on top.

For those experiments including temperature measurements the eruptions tended to take place at or close to a sensor drill hole. In experiments without temperature sensors the weak spot was random. In one extended experiment a vertical tunnel formed towards the surface.

As pointed out above, the reproducibility of temperature profile measurements was very much affected by latent heat release, although the sensors positioned at or closest to the dust layer generally recorded a temperature increase higher than the temperature increase recorded approximately 1 cm above the dust layer. However, no sub-surface temperature maximum that would prove the SSGE in CO_2 ice could be measured.

We did not observe that channels formed in the course of an experiment closed again due to CO_2 re-deposition, as described in a theoretical model by Portyankina et al., (2010). However, in their model they used much smaller particle sizes and thicker ice layers ($r \leq 8$ µm, $h = 1$ m). Our experiments however, were limited to relatively small samples and short timescales and, perhaps most importantly, were limited to one insolation cycle. It would be interesting to observe whether any channels could be closed by CO_2 re-deposition during a cooling cycle.

Whether dust erupts on Mars may depend on the thickness, the compactness and transparency of the ice layer above the dust as well as the grain size of the dust. Using the facilities in the laboratory limits the size of the single samples and therefore the thickness of the ice layer above the embedded dust.

CO_2 geysers have been proposed as the source for some of the enigmatic features in Mars' cryptic region. In order for this hypothesis to work, there needs to be a pressure difference between CO_2 gas trapped beneath the ice and the atmosphere. Obtaining this specific pressure difference under laboratory conditions is extremely difficult because the thermodynamic response times in an environmental chamber on Earth are a lot shorter than they are on Mars.

Acknowledgements

The authors would like to acknowledge Stephen Wolters' assistance with sample preparation. This project was funded by the UK Space Agency under Grant No. ST/J005304/1 with additional support from STFC (grant no. ST/L000776/1). The authors would like to thank two anonymous reviewers for their helpful suggestions which greatly improved this paper.

References

Behn, U., 1900. In: Ueber Die Dichte Der Kohlensäure Im Festen Und Flüssigem Zustande, Vol. 308. Annalen der Physik, p. 112.

Bibring, J.P., Langevin, Y., Poulet, F., Gendrin, A., Gondet, B., Berthe, M., Soufflot, A., Drossart, P., Combes, M., Bellucci, G., Moroz, V., Mangold, N., Schmitt, B., 2004. Perennial water ice identified in the south polar cap of Mars. Nature 428, 627–630.

Brown, R.H., Matson, D.L., 1987. Thermal effects of insolation propagation into the regoliths of airless bodies. Icarus 72, 84–94.
Dissly, R., Brown, R.H., Matson, D.L., 1990. Laboratory measurements of the solid-state greenhouse effect in glass beads. In: Abstracts of the Lunar and Planetary Science Conference, 21, p. 295.
de Villiers, S., Nermoen, A., Jamtveit, B., Mathiesen, J., Meakin, P., Werner, S.C., 2012. Formation of Martian araneiforms by gas-driven erosion of granular material. Geophys. Res. Lett. 39, L13204. doi:10.1029/2012GL052226.
Fanale, F.P., Salvail, J.R., Matson, D.L., Brown, R.H., 1990. The effect of volume phase changes, mass transport, sunlight penetration, and densification on the thermal regime of icy regoliths. Icarus 88, 193–204.
Hansen, C.J., Thomas, N., Portyankina, G., McEwen, A., Becker, T., Byrne, S., Herkenhoff, Kieffer, K.H., Mellon, M., 2010. HiRISE observations of gas sublimation–driven activity in Mars' southern polar regions: I. Erosion of the surface. Icarus 205, 283–295.
Kaufmann, E., Kömle, N.I., Kargl, G., 2006. Laboratory simulation experiments on the solid-state greenhouse effect in planetary ices. Icarus 185, 274–286.
Kieffer, H.H., Titus, T.N., Mullins, K.F., 2000. Mars south polar spring and summer behavior observed by TES: seasonal cap evolution controlled by frost grain size. J. Geophys. Res. 105 (E4), 9643–9699.
Kieffer, HughH., Christensen, PhilipR., Titus, TimothyN., 2006. CO_2 jets formed by sublimation beneath translucent slab ice in Mars' seasonal south polar ice cap. Nature 442. doi:10.1038/nature04945, 17 August 2006.
Langevin, Y., Poulet, F., Bibring, J.-P., Schmitt, B., Doute, S., Gondet, B., 2005. Summer evolution of the north polar cap of Mars as observed by OMEGA/Mars express. Science 307, 1581–1584.
Langevin, Y., Douté, S., Vincendon, M., Poulet, F., Bibring, J.P., Gondet, B., Schmitt, B., Forget, F., 2006. No signature of clear CO_2 ice from the "cryptic" regions in Mars' south seasonal polar cap. Nature 442, 790–792.
Matson, D.L., Brown, R.H., 1989. Solid-state greenhouses and their implication for icy satellites. Icarus 77, 67–81.
Meyers, C.H., Van Dusen, M.S., 1933. The vapor pressure of liquid and solid carbon dioxide. Bureau Stand. J. Res. 10.
Paige, D.A., Keegan, K.D., 1994. Thermal and albedo mapping of the polar regions of Mars using viking thermal mapper observations, 2, south polar region. J. Geophys. Res. 99, 25993–26014.
Paige, D.A., Bachman, J.E., Keegan, K.D., 1994. Thermal and albedo mapping of the polar regions of Mars using viking thermal mapper observations, 1, North polar region. J. Geophys. Res. 99, 25959–25992.
Philippe, S., Schmitt, B., Beck, P., Brissaud, O., 2015. Thermal cracking of CO_2 slab ice as the main driving force for albedo increase of the martian seasonal polar caps. EPSC2015-111, European Planetary Science Congress 2015, held 27 September - 2 October 2015 in Nantes, France.
Piqueux, S., Byrne, S., Richardson, M.I., 2003. Sublimation of Mars's southern seasonal CO_2 ice cap and the formation of spiders. J. Geophys. Res. 108 (E8), 5084.
Portyankina, G., Markiewicz, W.J., Hansen, C.J., Thomas, N., 2010. HiRISE observations of gas sublimation-driven activity in Mars' southern polar regions: III. Models of processes involving translucent ice. Icarus 205, 311–320.
Portyankina, G., Pommerol, A., Aye, K., Hansen, C.J., Thomas, N., 2012. Polygonal cracks in the seasonal semi-translucent CO_2 ice layer in martian polar areas. J. Geophys. Res. 117, E02006.
Soderblom, L.A., Becker, T.L., Kieffer, S.W., Brown, R.H., Hansen, C.J., Johnson, T.V., 1990. Triton's geyser-like plumes - Discovery and basic characterization. Science 250, 410–415.
Thomas, N., Hansen, C.J., Portyankina, G., Russell, P.S., 2010. HiRISE observations of gas sublimation-driven activity in Mars' southern polar regions: II. Surficial deposits and their origins. Icarus 205 (1), 296–310.
Titus, T.N., Calvin, W.M., Kieffer, H.H., Langevin, Y., Prettyman, T.H., July 2008. Martian Polar Processes 578–+, (Chapter 25).